Environmental Science & Technology

pubs.acs.org/est

Article

Direct Evidence of a Light-Dependent Sink of Superoxide within Chromophoric Dissolved Organic Matter

Danielle M. Le Roux, Leanne C. Powers, and Neil V. Blough*

Cite This: *Environ. Sci. Technol.* 2023, 57, 20627−20635

Read Online

ACCESS | Metrics & More | Article Recommendations | Supporting Information

Downloaded via UNIV OF GEORGIA on September 2, 2024 at 16:36:55 (UTC).
See https://pubs.acs.org/sharingguidelines for options on how to legitimately share published articles.

ABSTRACT: Superoxide ($O_2^{\bullet -}$) is produced photochemically in natural waters by chromophoric dissolved organic matter (CDOM) via the reaction of molecular oxygen with photoproduced one-electron reductants (OERs) within CDOM. In the absence of other sinks (metals or organic radicals), $O_2^{\bullet -}$ is believed to undergo primarily dismutation to produce hydrogen peroxide (H_2O_2). However, past studies have implicated the presence of an additional light-dependent sink of $O_2^{\bullet -}$ that does not lead to H_2O_2 production. Here, we provide direct evidence of this sink through $O_2^{\bullet -}$ injection experiments. During irradiations, spikes of $O_2^{\bullet -}$ are consumed to a greater extent (∼85−30% loss) and are lost much faster (up to ∼0.09 s^{-1}) than spikes introduced post-irradiation (∼50−0% loss and ∼0.03 s^{-1} rate constant). The magnitude of the loss during irradiation and the rate constant are wavelength-dependent. Analysis of the H_2O_2 concentration post-spike indicates that this light-dependent sink does not produce H_2O_2 at low spike concentrations. This work further demonstrates that simply assuming that the $O_2^{\bullet -}$ production is twice the H_2O_2 production is not accurate, as previously believed.

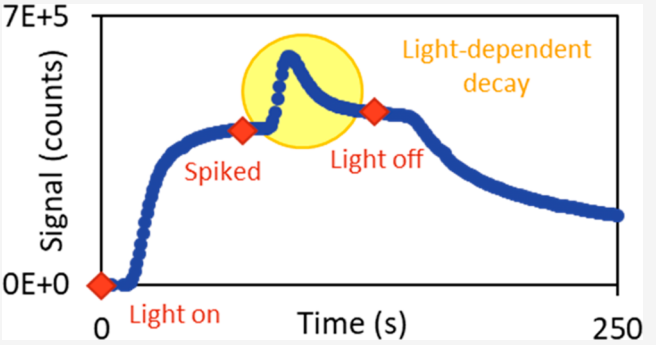

KEYWORDS: *photodegradation, irradiation, superoxide decay pathways, decay modeling*

INTRODUCTION

Chromophoric dissolved organic matter (CDOM) absorbs sunlight to produce a variety of reactive oxygen species (ROS) in natural waters.[1−5] One of these ROS is superoxide ($O_2^{\bullet -}$), which is produced primarily when CDOM is promoted to excited singlet states, which then undergo one-electron transfer between donor and acceptor groups to produce one-electron reductants (OERs).[6−8] These OERs then react with dissolved molecular oxygen to produce $O_2^{\bullet -}$.[6,7] Possible decay pathways for $O_2^{\bullet -}$ in natural waters involve reactions with metals,[9−13] dissolved organic matter (DOM) itself,[14,15] organic radicals,[16−18] and dismutation to form hydrogen peroxide (H_2O_2).[19]

H_2O_2, as a product of $O_2^{\bullet -}$ dismutation, has been employed as a proxy for $O_2^{\bullet -}$ production as a result of its stability and ease of measurement.[20−22] The assumption usually made is that $O_2^{\bullet -}$ production is double the H_2O_2 production on the basis of the stoichiometry of dismutation (catalyzed or uncatalyzed).[14,23] However, using the enzyme superoxide dismutase (SOD) to catalyze the dismutation of $O_2^{\bullet -}$ to H_2O_2, a discrepancy was noted between the rates of production of $O_2^{\bullet -}$ and H_2O_2 in the presence of SOD. SOD caused the rates of H_2O_2 production to increase, suggesting that a significant portion of $O_2^{\bullet -}$ produced was lost through a competitive pathway that did not lead to H_2O_2.[20−22,24]

Direct measurements of the production of $O_2^{\bullet -}$ have been made and compared to H_2O_2 measurements. Currently, the most widely used method is based on a chemiluminescent reaction employing flow injection analysis that allows for continuous measurement of $O_2^{\bullet -}$.[25] During an irradiation, the establishment of a steady state can be observed, while the dark decay can be monitored following the removal of light.[24,26,27] The production rate can then be calculated from the steady-state concentration and dark decay rate constant, assuming that the dark decay rate is the total decay rate. The stoichiometry of the reaction for dismutation should result in a ratio of $O_2^{\bullet -}/H_2O_2$ rates equal to 2. However, values of 2.2−9.8 have been obtained for various natural waters suggesting that an oxidative reaction is competing with dismutation.[28]

Alternatively, some studies have directly measured the initial production rate and compared this to the calculated production rate obtained from the dark decay and steady-state concentration.[28−30] Powers et al.[28] found that the

Received: October 5, 2023
Revised: November 12, 2023
Accepted: November 13, 2023
Published: December 4, 2023

ACS Publications

© 2023 American Chemical Society

modeled rates were similar to the measured initial rates for samples from the Gulf of Alaska. Shaked et al.[29] also claimed to have obtained similar results for the Gulf of Aqaba, but their measured initial rates are slightly higher than the range of their modeled rates. Ma et al.[30] found that the measured initial rates were 2−5 times higher compared to the modeled rates for a variety of reference materials and wastewater effluents. Issues with quantifying initial rates have been raised and include the unavoidable loss of $O_2^{\bullet -}$ during the transit time from the sample to the detector, which Ma et al. attempted to account for using a correction procedure.[28−30] An additional issue is that the choice of the time range over which the initial rate is measured can heavily influence the values.[28,29] Regardless, the fact that measured production rates have been observed to be larger than calculated production rates suggests that a kinetic model using only the dark decay rate constant leads to an underestimation of the production rates, implying the presence of an additional decay pathway for $O_2^{\bullet -}$. Because the observed dark decay of $O_2^{\bullet -}$ is the culmination of possible dark decay pathways, the additional pathway that is not being observed in the dark would be some light-dependent decay pathway.

Because $O_2^{\bullet -}$ is rather difficult to measure experimentally, recent work has studied the production rates of the OER, the proposed precursor to $O_2^{\bullet -}$.[6−8] OER production has recently been compared to $O_2^{\bullet -}$ production, and the rates were similar in magnitude, suggesting that the measurement of OER may currently be the best proxy for $O_2^{\bullet -}$. OER values have therefore been compared to H_2O_2 production. Theoretically, a value of 2 should also be obtained here as well, but values from 5 to 16 have been observed in reference materials, exudates, natural waters, and C-18 extracts, again suggesting the presence of an additional pathway for $O_2^{\bullet -}$ loss.[7,8] The culmination of these results suggests that there is an additional light-dependent oxidative sink for $O_2^{\bullet -}$ that does not lead to H_2O_2 production. Therefore, current decay models used for $O_2^{\bullet -}$ do not accurately reflect the magnitude of the total decay. This leads to an underestimation of the level of production of $O_2^{\bullet -}$ as determined from the steady-state concentration and dark decay data. It has been suggested that a light-dependent sink exists that is associated with CDOM, but very little work has been done to investigate this possibility. Work reported by Ma et al. attempted to determine the light-dependent decay rate constant.[30] The initial production rate of $O_2^{\bullet -}$ was divided by the steady-state concentration to calculate a total first-order decay rate constant. This rate constant represents a combination of the light-dependent decay, decay as a result of dismutation, and other possible pseudo-first-order decay pathways. The light-dependent decay rate constant was then determined by subtracting the rate constants for dismutation and the dark pseudo-first-order decay. The light-dependent decay rate constants were found to be in the range of 0.1−0.4 s^{-1}, which constituted between 63 and 81% of the overall decay constant.[30]

However, direct evidence of the presence of this sink does not yet exist. Here, we directly demonstrate the existence of this sink through spiking experiments.[31] When a sample is at a steady state during an irradiation, the sample is injected with an aliquot of $O_2^{\bullet -}$, and the loss and decay of $O_2^{\bullet -}$ is monitored. For comparison, the sample is also spiked during the decay phase, when the sample was removed from light. This work demonstrates that $O_2^{\bullet -}$ is consumed rapidly when the light is on compared to the much slower decay that occurs when the light is off. Significant quantitative work and modeling of the data have been conducted to directly determine the light-dependent rate constant. These values can be used to modify existing decay models to provide better estimates of $O_2^{\bullet -}$ production rates.

MATERIALS AND METHODS

Chemicals. Boric acid, sodium acetate, sodium carbonate, monobasic sodium phosphate, hydrochloric acid (HCl), sodium hydroxide (NaOH), phosphoric acid, and superoxide dismutase (SOD, from bovine erythrocytes) were purchased from Millipore Sigma. Acetone and ethanol were purchased from Fisher Scientific. All reagents/chemicals were ACS-grade. 2-Methyl-6-(4-methoxyphenyl)-3,7-dihydroimidazo[1,2-*a*]-pyrazin-3(7*H*)-one) (methyl *Cypridina* luciferin analogue or MCLA) was purchased from TCI Chemicals. Diethylene-triaminepentaacetic acid (DTPA) was purchased from Fluka. 10-Methyl-9-(*p*-formylphenyl)acridinium carboxylate trifluor-omethanesulfonate (acridinium ester or AE) was purchased from Waterville Analytical Co. Hydrogen peroxide (H_2O_2) was purchased from EMD. Suwannee River fulvic acid (SRFA, 3S101F) was purchased from the International Humic Substance Society. Purified water (18 MΩ cm) was obtained from a Sartorius Arium Mini purification system.

Sample Preparation. Stock solutions of SRFA were prepared by diluting and dissolving SRFA in ultrapure water. These stocks were adjusted to pH 7 using NaOH and HCl and filtered using pre-cleaned 0.2 μM nylon filters. Dilutions of these stocks at desired concentrations for experiments were then prepared by diluting the stock solutions with 50 mM borate buffer at a pH of 8.0 ± 0.1.

Measurement of Superoxide. $O_2^{\bullet -}$ was measured in a FeLume system by Waterville Analytical Co. via reaction with the chemiluminescent reagent MCLA.[25] The voltage of the photomultiplier tube (PMT) was operated at 1000 V, and the integration time was 800 ms. A peristaltic pump was used to continuously pump the reagent and sample into the instrument and was operated at 25.5 rpm (total flow rate of 6.6 mL/min). MCLA was prepared at 2.5 μM in 500 mM sodium acetate buffer with 50 μM DTPA at a pH of 6.[25] Stocks of $O_2^{\bullet -}$ were generated by photolysis of a solution of 6 M ethanol, 41 mM acetone, and 30 μM DTPA in 1 mM borate buffer at a pH of 12.5 in a cuvette with a mercury pen lamp.[25,32] The stock concentration was monitored spectrophotometrically (ε = 2183 M^{-1} cm^{-1} at 240 nm)[33] with an Ocean Insight DH mini light source connected to an Ocean Optics USB2000 spectrometer. Upon reaching ∼50 μM $O_2^{\bullet -}$, a small volume (μL) was taken and added to ∼20 mL of sample to prepare a standard in the nanomolar range. The standards were continuously stirred using a magnetic stir bar and stir plate, and the signal was monitored as $O_2^{\bullet -}$ decayed. Linear extrapolation of the plot of the natural log of the signal versus time was used to determine what the initial signal was for generation of calibration curves.

Measurements of the photoproduction of $O_2^{\bullet -}$ were conducted in a 5 cm path length quartz cylindrical cell (15 mL total volume). The sample line was placed in the cell, and the cell was irradiated. A 300 W xenon arc lamp was used for irradiations along with a 20 cm water jacket and various long-pass cutoff filters (325, 355, 380, 399, 418, and 440 nm). The sample was monitored to acquire the time course of $O_2^{\bullet -}$ production and the establishment of a steady state, with the cell then removed from the light to monitor the decay. For spiking experiments, a $O_2^{\bullet -}$ stock was generated as described

https://doi.org/10.1021/acs.est.3c08254
Environ. Sci. Technol. 2023, 57, 20627−20635

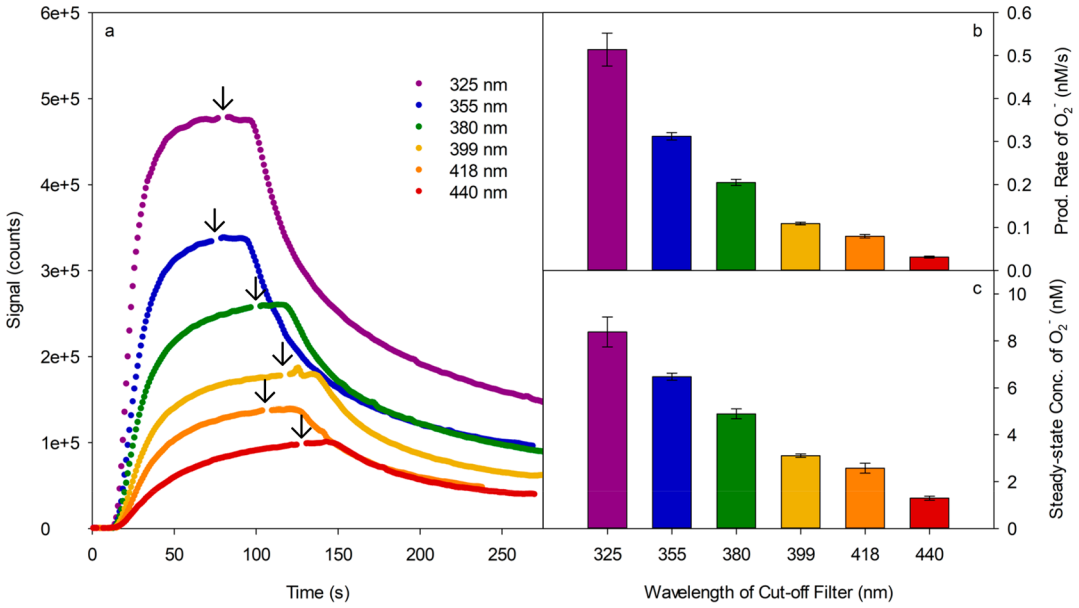

Figure 1. (a) Signals for $O_2^{\bullet -}$ production, establishment of a steady state, and decay of 1 mg/L SRFA, employing different wavelength cutoff filters. Irradiation was initiated at $t = 0$. Down arrows indicate removal of the sample from light. (b) Production rates and (c) steady-state concentrations were calculated on the basis of standard curves. Error bars are the standard deviation for three trials.

above and the sample was spiked with appropriate volumes of $O_2^{\bullet -}$ (low microliter range) during the steady-state phase or during the decay phase. The sample was continuously stirred using a stir bar and plate. Analysis of the data was primarily performed in Excel. Model fits of the baseline-corrected signals versus time were conducted in MATLAB using the curve fitting application.

Measurement of Hydrogen Peroxide. H_2O_2 was measured through the chemiluminescent reaction with AE in FeLume by Waterville Analytical Co. The carrier solution was 0.1 M HCl; the buffer was 0.1 M sodium carbonate at a pH of 11.7; and the reagent AE was prepared at 5 μM in 1 mM phosphate buffer at a pH of 3.[34,35] All of these solutions were drawn into the FIA system via Teflon tubing using a peristaltic pump. The PMT was set at a voltage of 950 V with an integration time of 400 ms.

Standards of H_2O_2 were prepared from a stock solution whose concentration was monitored spectrophotometrically (ε = 38.1 ± 1.4 M^{-1} cm^{-1} at 240 nm).[36] To determine the concentration of H_2O_2 in a sample, the sample was irradiated using the lamp, water jacket, and filters, as described above. H_2O_2 irradiations were conducted in a 3 cm cubic quartz cell as a result of the need to do this analysis on a higher concentration of SRFA (10 mg/L) because of the lower sensitivity of the H_2O_2 method. An aliquot of the sample was taken and injected into the instrument for analysis when needed. The concentration was then determined using the obtained signal and the standard curve.

Absorbance and Fluorescence Measurements. Absorbance measurements were conducted on a Shimadzu UVPC 2401 benchtop spectrophotometer. The instrument was baselined to air, and blank measurements (ultrapure water or buffer) were taken and subtracted from absorbance spectra. Fluorescence excitation−emission spectra (EEMs) were conducted with a Horiba FluoroMax 4. Excitation was scanned from 300 to 500 nm every 10 nm, and the emission was scanned from 300 to 700 nm every 1 nm. Band passes were 4 nm, and the integration time was 0.2 s. First- and second-order Rayleigh masking settings in the program were used.

RESULTS AND DISCUSSION

Wavelength Dependence of Superoxide Data. Upon irradiation of 1 mg/L SRFA, the $O_2^{\bullet -}$ concentration rises rapidly and approaches a steady state within approximately 1−2 min, depending upon the wavelength of the cutoff filter used (Figure 1). As the wavelength of the cutoff filter was increased, the rates of production of $O_2^{\bullet -}$ and the steady-state concentrations decreased. Initial $O_2^{\bullet -}$ production rates were determined on the basis of ∼15 s of data following the delay time (delay from initiation of irradiation to detection) with no correction for any losses (for simplicity of demonstrating and using raw data). Steady-state concentrations were calculated by the average of ∼10 points of the plateau, near the time that the sample was removed from the light, with no correction for losses as a result of the delay time. The decay of $O_2^{\bullet -}$ is observed following the removal of the sample from the light (see in-depth kinetic analysis below for more information). Very little data exists in the literature concerning the wavelength dependence of the time courses for the photochemical formation and decay of $O_2^{\bullet -}$, although several studies have estimated formation rates based on H_2O_2 data.[22,27] Our results demonstrate that the production rate and steady-state concentration decrease with an increasing wavelength of the cutoff filter, consistent with a limited number of studies on $O_2^{\bullet -}$.[8,30]

The dark decay rate was observed to be significantly slower in the presence of DTPA when $O_2^{\bullet -}$ was injected into the buffer and SRFA solutions alone (Text S1 and Figures S1 and S2 of the Supporting Information), suggesting that metal-catalyzed dismutation of $O_2^{\bullet -}$ might be contributing to the dark decay rate. However, because of our concerns that DTPA would interfere with the light-dependent studies, it was not included in these experiments (Text S1 of the Supporting Information). Additionally, not including DTPA allowed for the study of the $O_2^{\bullet -}$ reactions under more natural conditions.

https://doi.org/10.1021/acs.est.3c08254
Environ. Sci. Technol. 2023, 57, 20627−20635

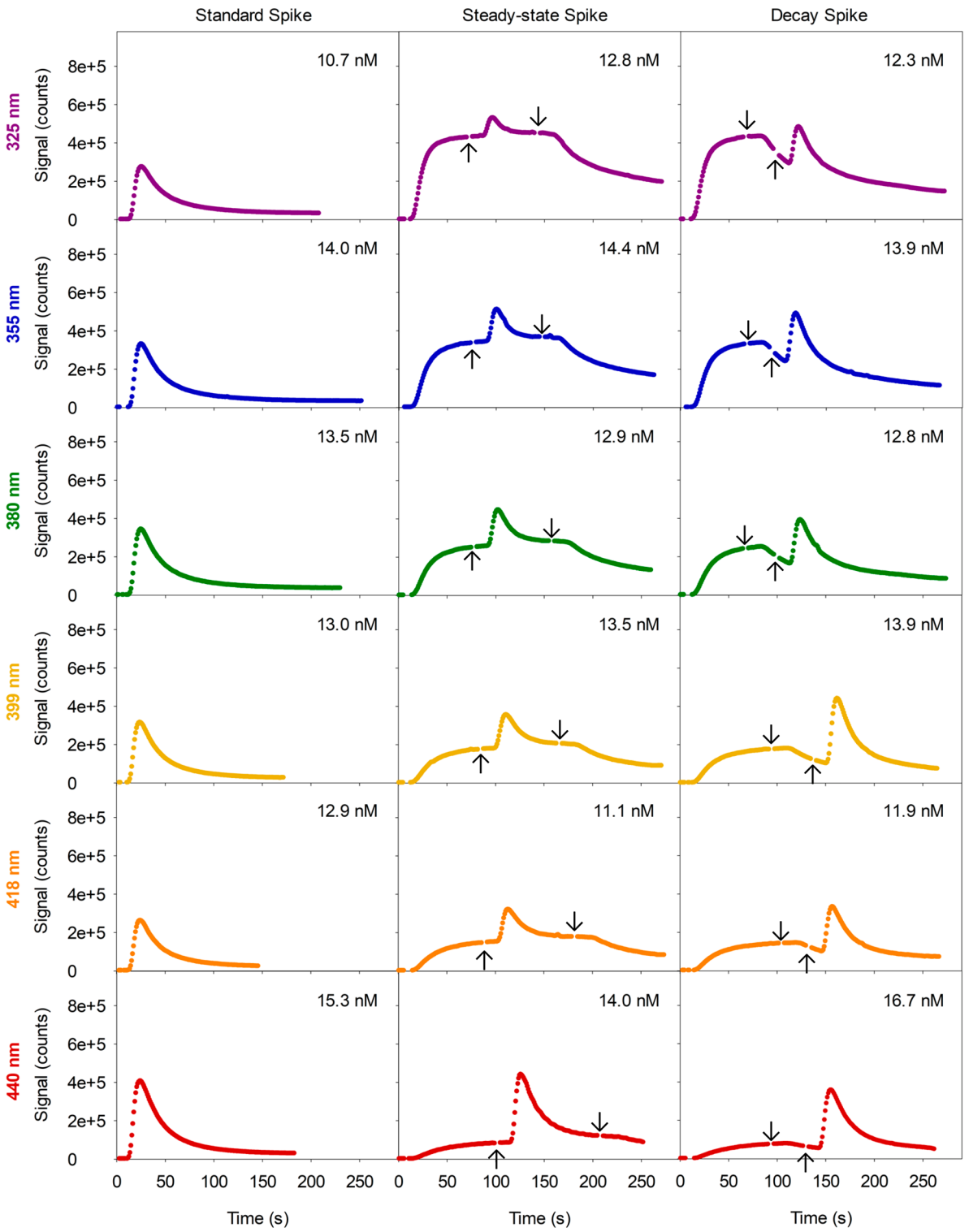

Figure 2. Time courses of $O_2^{\bullet -}$ following injection: Left column, 1 mg/L SRFA in the dark; middle column, injection at a steady state; and right column, injection post-irradiation. Colors indicate the wavelength of the cutoff filter used. For all columns, irradiation was initiated at $t = 0$. Up-facing arrows indicate the time of the $O_2^{\bullet -}$ injection, and down-facing arrows indicate the time that the sample was removed from light. Final concentrations of injected $O_2^{\bullet -}$ are in the upper right of the panels.

Observance of the Enhanced Decay of Superoxide during Irradiation. Spiking experiments were conducted in which $O_2^{\bullet -}$ was injected into 1 mg/L SRFA solutions during irradiation and during the decay post-irradiation (Figure 2). Standard spikes of $O_2^{\bullet -}$ into SRFA in the dark are also shown, with the concentrations of the spikes approximately matched (left panels in Figure 2). When the magnitudes of the signals observed for the standard spikes and the spikes introduced at a steady state are compared, a substantial reduction in the amplitude of the steady-state spikes was observed at shorter wavelengths as well as a more rapid decay of remaining $O_2^{\bullet -}$ (discussed at length in the kinetic section below). This

https://doi.org/10.1021/acs.est.3c08254
Environ. Sci. Technol. 2023, 57, 20627−20635

behavior provides evidence that a significant fraction of $O_2^{\bullet -}$ is consumed in the light at a rate that we cannot resolve kinetically, particularly for the shorter wavelength cutoff filters. In contrast, the magnitudes of the signals observed for the $O_2^{\bullet -}$ injections post-irradiation (during decay) were significantly larger and closer to those observed for the standard spikes. Below, we first quantify the loss of $O_2^{\bullet -}$ following injections at both a steady state and post-irradiation, followed by an analysis of the kinetics of $O_2^{\bullet -}$ decay.

Quantification of Superoxide Loss Following Steady-State and Post-irradiation Spikes. To quantify the loss of $O_2^{\bullet -}$ in the steady-state and post-irradiation spikes (middle and right columns, respectively, in Figure 2), their peak heights were compared to that of the standards (left column in Figure 2 and Text S2 of the Supporting Information). Steady-state spikes exhibited a substantial loss of $O_2^{\bullet -}$, ranging from ∼30% of the injected $O_2^{\bullet -}$ concentration with the 440 nm cutoff filter to ∼85% with the 325 nm filter (Figure 3); these

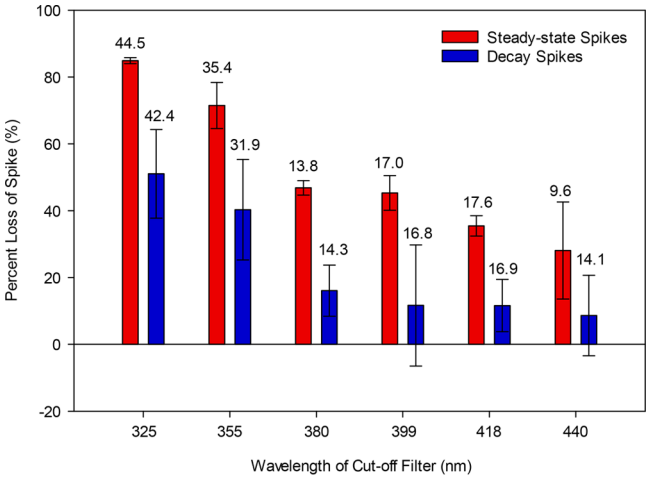

Figure 3. Percent loss of steady-state and post-irradiation spikes in 1 mg/L SRFA for each wavelength cutoff filter. Error bars are the standard deviation of at least three injections. Values above the bars are the $O_2^{\bullet -}$ concentrations (nM) of the largest injected spikes for the cutoff filters.

percentages correspond to consumed $O_2^{\bullet -}$ concentrations ranging from ∼10 to ∼40 nM using 1 mg/L SRFA. Thus, a more substantial loss of $O_2^{\bullet -}$ was observed under irradiation with the shorter wavelength cutoff filters, necessitating the use of larger spike concentrations to observe a residual signal.

In contrast, the losses of $O_2^{\bullet -}$ in the post-irradiation spikes were substantially smaller, ranging from no detectable loss with the 418 and 440 nm filters to ∼50% of the injected $O_2^{\bullet -}$ concentration with the 325 nm filter, corresponding to a consumed $O_2^{\bullet -}$ concentration of ∼20 nM. The observation that the post-irradiation $O_2^{\bullet -}$ losses were substantial with the shorter wavelength cutoff filters suggests that longer lived, photoproduced intermediates reactive with $O_2^{\bullet -}$ remain following irradiation at the shorter wavelengths.[37]

Kinetic Analysis of the $O_2^{\bullet -}$ Decay Data. First- and second-order fits were applied to the decay data to examine which kinetic model best represented the data. Because the decays slowed considerably at longer times and never reached baseline in any of the decays, a constant offset was included as a variable in the first- and second-order fits to account for this small residual signal (Text S3 of the Supporting Information). Including this offset significantly improved the fits. Goodness of fit was determined on the basis of R^2 values as well as consistency between the known spike concentration and concentration of $O_2^{\bullet -}$ acquired from the fit extrapolated to the injection time.

Fits were applied to the dark decay of $O_2^{\bullet -}$ in SRFA, the post-irradiation decay (PID), the decay in the dark post-steady-state spike (PSD), the decay phase spike (DSD), and the steady-state spike decay (SSD) (Figure 4 and Text S4 of

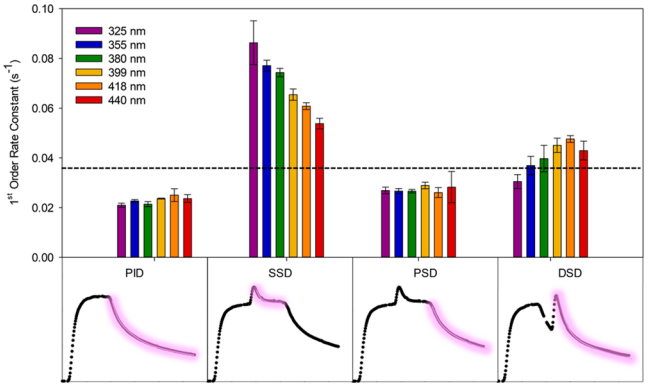

Figure 4. First-order fits to post-irradiation decay (PID), steady-state spike decay (SSD), post-steady-state spike decay (PSD), and decay phase spike decay (DSD) for all wavelength cutoff filters. Dashed lines indicate the average rate constant obtained for the standard dark decay (∼0.037 s^{-1}). The bottom panel shows a visual for the data that were fit for each category. Error bars are standard deviations for fits to at least three trials.

the Supporting Information). A first-order model provided the best fits to the SSD and DSD and, surprisingly, to the dark decay of $O_2^{\bullet -}$ in SRFA (0.037 ± 0.002 s^{-1}; Figures S7 and S8 of the Supporting Information). A second-order model appeared to fit PID and PSD the best (Figure S9 of the Supporting Information). For ease of comparison, the discussion here focuses on all first-order fits. More information can be found in the Supporting Information regarding the second-order fits (Text S4 of the Supporting Information). First-order rate constants acquired from fits to the SSD were substantially larger than that for the dark decay of $O_2^{\bullet -}$ in SRFA, ranging from 0.086 ± 0.009 s^{-1} with the 325 nm filter to 0.054 ± 0.002 s^{-1} with the 440 nm filter, further demonstrating an enhanced rate of loss of $O_2^{\bullet -}$ under irradiation (Figure 4). The first-order fits and rate constants acquired from the dark decay fits were independent of the injected $O_2^{\bullet -}$ concentration over the range from ∼5 to 30 nM (Figure S10 of the Supporting Information).

The SSD rate constant for the 325 nm cutoff filter is similar in magnitude but slightly smaller than that recently calculated by Ma et al.[30] from data acquired with a 290 nm cutoff filter (∼0.12 s^{-1}). However, for filter wavelengths of ≥380 nm, extrapolation of the first-order fits of the SSD to the injection time (t = 0) provided concentrations of $O_2^{\bullet -}$ that are slightly greater than or similar in magnitude to the expected concentrations (on the basis of the known injection volumes and stock concentrations), but the extrapolated time zero concentrations were substantially smaller than the expected concentrations with the 325 nm filter (Table S1 of the Supporting Information). This result implies that shorter wavelength irradiation with the 325 nm filter produces an

https://doi.org/10.1021/acs.est.3c08254
Environ. Sci. Technol. 2023, 57, 20627−20635

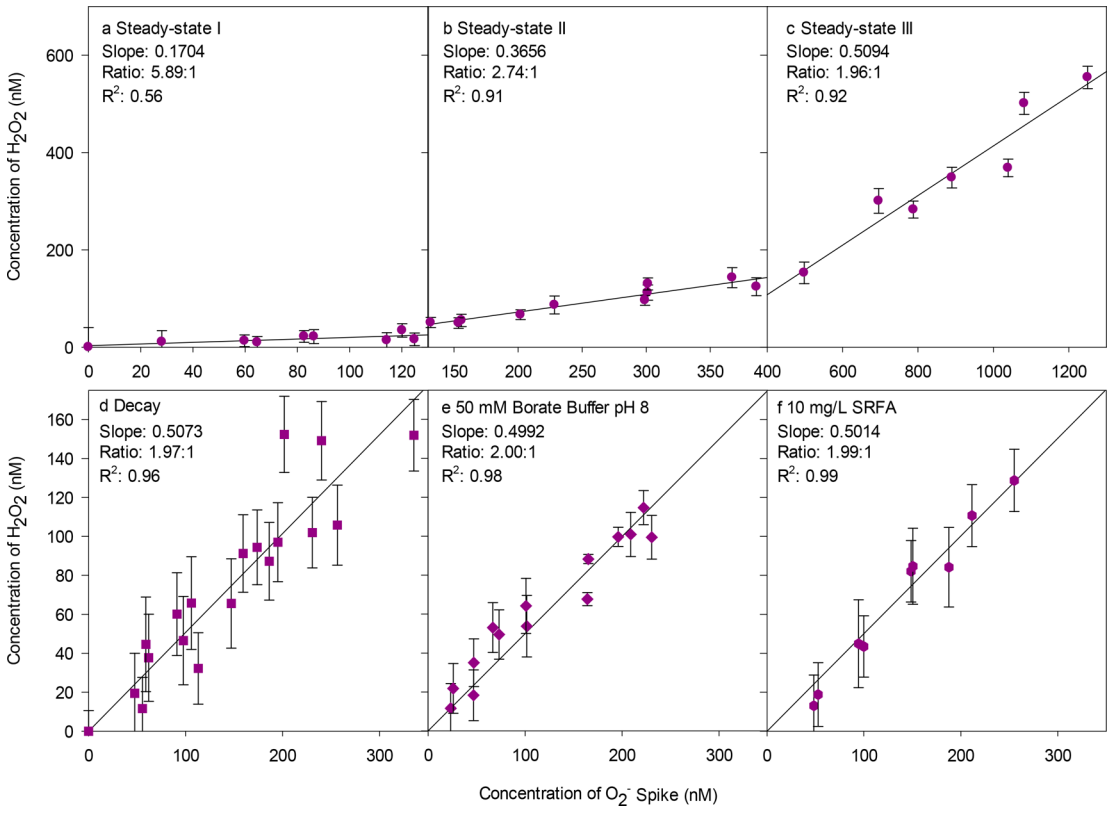

Figure 5. Concentration of H_2O_2 produced from $O_2^{\bullet -}$ spikes injected (a–c) at a steady state, (d) during decay, (e) in the dark in 50 mM borate buffer at pH 8, and (f) in the dark in 10 mg/L SRFA. Irradiations were done with the 325 nm cutoff filter. Photoproduced H_2O_2 was subtracted from the data. Steady-state spikes were split into three regions to emphasize the changes in the slope. Ratio values are the inverse of the slope and are therefore the ratio of H_2O_2 produced to $O_2^{\bullet -}$ injected. Error bars are for standard deviation of triplicate measurements post-spike.

additional, more rapid pathway for $O_2^{\bullet -}$ loss that we cannot resolve kinetically.

In contrast to the SSD, the rate constants for the DSD were less dependent upon the irradiation wavelength and were significantly smaller (~0.04 s^{-1}), with values similar to the rate constant for dark decay in SRFA (0.037 s^{-1}), further confirming that the sink is light-dependent. The first-order rate constants determined for PID and PSD data were very similar to values in the range of 0.020–0.029 s^{-1} across the different wavelength filters (Tables S1–S6 of the Supporting Information), which indicates that the injection of $O_2^{\bullet -}$ during a steady state had no impact on the post-spike dark decay. Additionally, PID and PSD rate constants were up to ~2-fold smaller than the first-order rate constant determined for dark decay of $O_2^{\bullet -}$ in SRFA (~0.037 s^{-1}) as well as those of the DSD (Figure 4). The phenomenon of a slower dark decay following irradiation has been observed in previous studies with various explanations for its origins (Text S4 of the Supporting Information).[28,38,39] Garg et al. suggested that the dark decay pathway(s) were deactivated or modified during irradiation.[24] Our observation that the kinetics are altered following irradiation (in terms of either first versus second order or differences in magnitude in first-order rate constants; Figure 4) would appear to support this idea but would be surprising given the very short (<4 min) irradiation time.

Hydrogen Peroxide Concentration Post-spike. $O_2^{\bullet -}$ has been shown to be primarily formed from the photoproduction of OERs within CDOM.[6−8] The possibilities for a light-dependent sink for $O_2^{\bullet -}$ are as follows: (1) back reaction with the oxidized group within CDOM to reform molecular oxygen, (2) reaction with the oxidized group within CDOM, with further intramolecular reactions potentially leading to ring-opened products, (3) reduction to form H_2O_2, or (4) another oxidation reaction leading to molecular oxygen.

$$CDOM^{\bullet +} + O_2^{\bullet -} \rightarrow CDOM + O_2 \quad (1)$$

$$CDOM^{\bullet +} + O_2^{\bullet -} \rightarrow CDOM{-}O_2 \rightarrow \text{intramolecular reactions} \quad (2)$$

$$CDOM^{red} + O_2^{\bullet -} \rightarrow CDOM + H_2O_2 \quad (3)$$

$$CDOM^{ox} + O_2^{\bullet -} \rightarrow CDOM + O_2 \quad (4)$$

Although the available evidence indicates that this sink does not produce H_2O_2,[7,8,21,22,30] this possibility was further tested by measuring the H_2O_2 production after the introduction of $O_2^{\bullet -}$ spikes. H_2O_2 concentrations were analyzed following injections of $O_2^{\bullet -}$ at a steady state, during post-irradiation decay, and in non-irradiated samples in the dark. Because our detection limit was significantly higher for H_2O_2 than $O_2^{\bullet -}$ (~60×, as previously determined),[8] 10 mg/L SRFA was employed in place of 1 mg/L SRFA used above for the $O_2^{\bullet -}$ experiments. The stoichiometry expected for $O_2^{\bullet -}$ dismutation is 2:1.[19] However, the stoichiometry for $O_2^{\bullet -}$ spikes introduced during irradiation were much greater than 2:1 for spike concentrations of ≤500 nM (Figure 5). For spike concentrations of ≤120 nM, a ratio of ~6:1 is obtained, indicating that at least 66% of $O_2^{\bullet -}$ is being consumed by this sink. For spike concentrations between 120 and 500 nM, a ratio of 2.7:1 is obtained, which indicates that about 27% of

https://doi.org/10.1021/acs.est.3c08254
Environ. Sci. Technol. 2023, 57, 20627−20635

$O_2^{\bullet -}$ is still being lost by this sink. At spike concentrations above 500 nM, a 2:1 ratio is observed (Figure 5). These results indicate that $O_2^{\bullet -}$ introduced during irradiation is being consumed by another pathway that is not leading to H_2O_2. The sink is largest at spike concentrations of ≤120 nM, indicating that the sink is smaller than this value for a 10 mg/L SRFA sample. At spike concentrations of >500 nM, dismutation appears to be the primary pathway for the decay of the $O_2^{\bullet -}$ decay.

Spikes introduced during the decay phase post-irradiation led to the expected 2:1 stoichiometry, which was also observed in the controls where $O_2^{\bullet -}$ spikes were introduced in the dark for both 10 mg/L SRFA and 50 mM borate buffer (Figure 5). Other groups have also observed a 2:1 stoichiometry of H_2O_2 production from $O_2^{\bullet -}$ spikes in various samples in the dark.[14,24] Garg et al.[24] further compared the dark results to irradiated conditions and noted that the H_2O_2 concentration did not increase much post-irradiation despite observable $O_2^{\bullet -}$ decay. They concluded that the decay occurring post-irradiation was not producing H_2O_2 and that catalyzed dismutation that occurs in the dark is possibly deactivated during irradiation. We monitored our spiked samples in the dark for an additional ∼5 min from the time the sample was tested for H_2O_2. We also observed no continual increases in the H_2O_2 concentration during this time for samples that had received either steady-state spikes or decay spikes (data not shown).

Possibilities for the Light-Dependent Oxidative Sink. As previously discussed,[7,8] moieties that could be involved in the one-electron transfer within CDOM are phenols as the donors and quinones as the acceptors. In this case, one-electron transfer would result in the formation of phenoxy radicals, which have rate constants for reaction with $O_2^{\bullet -}$ near the diffusion-controlled limit.[40] The reaction between phenoxy radicals and $O_2^{\bullet -}$ can lead to a back reaction to reform phenol and molecular oxygen via the addition of $O_2^{\bullet -}$ to the phenol ring; several studies have demonstrated that the ring addition reaction predominates.[41−44] Further reaction can produce ring-opened products.[41,43,44] This reaction sequence represents another possible pathway for the photochemical transformation of CDOM as it is transported from land to the open ocean. Currently, a key issue that remains is the branching ratio between the back reaction, which does not lead to CDOM transformation, and reactions leading to net oxidation (i.e., ring-opened products). Although it is not possible to track the remineralization of CDOM to oxidized inorganic products (i.e., CO and CO_2) with this open-system experimental design, previous work suggests similar photoproduction efficiencies for CO_2 and $O_2^{\bullet -}$ based on a comparison between a CO_2 apparent quantum yield (AQY) spectrum and H_2O_2 AQY spectrum determined with added SOD.[27] However, only one coastal tidal creek sample was tested in this work, warranting further investigation into the relationship or lack thereof between $O_2^{\bullet -}$ and CO_2 photochemistry.

The possibility that $O_2^{\bullet -}$ is involved in the net oxidation of CDOM was tested preliminarily by measuring the absorbance and fluorescence before and after the injection of $O_2^{\bullet -}$ during irradiation. Small absorbance changes were observed between the wavelengths (200−450 nm), amounting to about a 5% loss (Figure S12 of the Supporting Information). A more significant change was observed in the fluorescence intensity, where up to about a 15% loss was obtained (Figure S12 of the Supporting Information). The spiked sample was only irradiated for just under 3 min; therefore, any photochemically induced oxidation is likely insignificant in this time frame.[45] Because a fairly large spike concentration was employed (∼1250 nM), a large portion of this spike likely produced H_2O_2 (Figure 5). The absence of a more substantial loss in optical properties may be due to the injection of a single large pulse of $O_2^{\bullet -}$ into the sample. Regardless, the observation of optical changes supports the idea that $O_2^{\bullet -}$ does indeed react to chemically alter the CDOM during irradiation.

Although phenolic groups and quinones are large components of the antioxidant/free-radical scavenging capabilities of DOM,[46−48] most studies that have investigated this have only looked at their activity in the dark[46,48] or after removal from sunlight.[47] Irradiation of CDOM produces a variety of organic radicals, such as peroxy radicals, that could also be possible sinks for $O_2^{\bullet -}$, although past work suggests that peroxy radicals are not likely to be substantial sinks.[24] Methylhydroperoxide was the only short-chain peroxide to be observed in one study, but its production was an order of magnitude lower than that of H_2O_2.[49]

■ ENVIRONMENTAL IMPORTANCE

We have demonstrated the presence of a light-dependent oxidative sink of $O_2^{\bullet -}$ within CDOM through $O_2^{\bullet -}$ spiking experiments. These results show that the simple assumption of the stoichiometric ratio of 2:1 for $O_2^{\bullet -}$ production based on H_2O_2 production is inaccurate and severely misrepresents the magnitude of $O_2^{\bullet -}$ photoproduction. On the basis of prior results,[6−8] the extent to which the photochemical formation of $O_2^{\bullet -}$ is undercalculated likely varies from sample to sample. Although only SRFA was studied here, this experimental approach should be applicable to a wide variety of samples to determine the magnitude of light-dependent oxidative consumption of $O_2^{\bullet -}$. However, considering that a wide variety of CDOM samples will likely have ratios larger than 2:1, any study that has utilized a value close to this ratio for modeling would likely need to be re-evaluated.[38,50] Future work should consider not only studying other humic and fulvic materials but also the influence of pH, salinity, ionic strength, and temperature.

Likely candidates for the moieties within CDOM that react with $O_2^{\bullet -}$ are photoproduced phenoxy radicals, which have large rate constants for reaction with $O_2^{\bullet -}$.[41] Past research has found that the reaction between $O_2^{\bullet -}$ and phenoxy radicals primarily occurs by addition followed by ring opening rather than regeneration of the parent phenol.[41,43,44] Our results support the idea that this process could be a contributing pathway for photo-oxidation of CDOM and, therefore, also possibly involved in the photoproduction of carbon dioxide and carbon monoxide. However, other additional possibilities for oxidative sinks exist, and the magnitude with which various pathways proceed over others is still currently unknown.

■ ASSOCIATED CONTENT

Supporting Information

The Supporting Information is available free of charge at https://pubs.acs.org/doi/10.1021/acs.est.3c08254.

Use of metal chelators in samples, details of data analysis, experiments using SOD, kinetic curve fitting process and tables of fit data, and changes in absorbance and fluorescence from spiking (PDF)

https://doi.org/10.1021/acs.est.3c08254
Environ. Sci. Technol. 2023, 57, 20627−20635

AUTHOR INFORMATION

Corresponding Author

Neil V. Blough − *Department of Chemistry and Biochemistry, University of Maryland, College Park, Maryland 20742, United States;* orcid.org/0000-0002-7938-4961; Email: neilb@umd.edu

Authors

Danielle M. Le Roux − *Department of Chemistry and Biochemistry, University of Maryland, College Park, Maryland 20742, United States;* orcid.org/0000-0003-2849-6856

Leanne C. Powers − *Department of Chemistry, State University of New York (SUNY) College of Environmental Science and Forestry, Syracuse, New York 13210, United States;* orcid.org/0000-0002-3538-7431

Complete contact information is available at: https://pubs.acs.org/10.1021/acs.est.3c08254

Notes

The authors declare no competing financial interest.

ACKNOWLEDGMENTS

This work was supported by grants from the National Science Foundation (NSF, OCE 1357411, OCE 1924595, and OCE 1924763).

REFERENCES

(1) Cooper, W. J.; Zika, R. G.; Petasne, R. G.; Fischer, A. M. Sunlight-Induced Photochemistry of Humic Substances in Natural Waters: Major Reactive Species. In *Aquatic Humic Substances*; Suffet, I. H., MacCarthy, P., Eds.; American Chemical Society (ACS): Washington, D.C., 1988; Advances in Chemistry, Vol. *219*, Chapter 22, pp 333−362, DOI: 10.1021/ba-1988-0219.ch022.

(2) Zika, R. G. Marine Organic Photochemistry. In *Marine Organic Chemistry—Evolution, Composition, Interactions and Chemistry of Organic Matter in Seawater*; Duursma, E. K., Dawson, R., Eds.; Elsevier: Amsterdam, Netherlands, 1981; Elsevier Oceanography Series, Vol. *31*, Chapter 10, pp 299−325, DOI: 10.1016/S0422-9894(08)70332-5.

(3) Zafiriou, O. C.; Joussot-Dubien, J.; Zepp, R. G.; Zika, R. G. Photochemistry of Natural Waters. *Environ. Sci. Technol.* **1984**, *18* (12), 358A−371A.

(4) Zika, R. G. Advances in Marine Photochemistry 1983−1987. *Rev. Geophys.* **1987**, *25* (6), 1390−1394.

(5) Blough, N. V.; Zepp, R. G. Reactive Oxygen Species in Natural Waters. In *Active Oxygen in Chemistry*; Foote, C. S., Valentine, J. S., Greenberg, A., Liebman, J. F., Eds.; Springer: Dordrecht, Netherlands, 1995; Structure Energetics and Reactivity in Chemistry Series (SEARCH Series), Vol. *2*, pp 280−333, DOI: 10.1007/978-94-007-0874-7_8.

(6) Zhang, Y.; Del Vecchio, R.; Blough, N. V. Investigating the Mechanism of Hydrogen Peroxide Photoproduction by Humic Substances. *Environ. Sci. Technol.* **2012**, *46* (21), 11836−11843.

(7) Zhang, Y.; Blough, N. V. Photoproduction of One-Electron Reducing Intermediates by Chromophoric Dissolved Organic Matter (CDOM): Relation to O_2^- and H_2O_2 Photoproduction and CDOM Photooxidation. *Environ. Sci. Technol.* **2016**, *50* (20), 11008−11015.

(8) Le Roux, D. M.; Powers, L. C.; Blough, N. V. Photoproduction Rates of One-Electron Reductants by Chromophoric Dissolved Organic Matter via Fluorescence Spectroscopy: Comparison with Superoxide and Hydrogen Peroxide Rates. *Environ. Sci. Technol.* **2021**, *55* (17), 12095−12105.

(9) Voelker, B. M.; Sedlak, D. L.; Zafiriou, O. C. Chemistry of Superoxide Radical in Seawater: Reactions with Organic Cu Complexes. *Environ. Sci. Technol.* **2000**, *34* (6), 1036−1042.

(10) Zafiriou, O. C.; Voelker, B. M.; Sedlak, D. L. Chemistry of the Superoxide Radical (O_2^-) in Seawater: Reactions with Inorganic Copper Complexes. *J. Phys. Chem. A* **1998**, *102* (28), 5693−5700.

(11) Garg, S.; Rose, A. L.; Waite, T. D. Superoxide-Mediated Reduction of Organically Complexed Iron(III): Impact of pH and Competing Cations (Ca^{2+}). *Geochim. Cosmochim. Acta* **2007**, *71* (23), 5620−5634.

(12) Garg, S.; Rose, A. L.; Waite, T. D. Superoxide Mediated Reduction of Organically Complexed Iron(III): Comparison of Non-Dissociative and Dissociative Reduction Pathways. *Environ. Sci. Technol.* **2007**, *41* (9), 3205−3212.

(13) Hansard, S. P.; Easter, H. D.; Voelker, B. M. Rapid Reaction of Nanomolar Mn(II) with Superoxide Radical in Seawater and Simulated Freshwater. *Environ. Sci. Technol.* **2011**, *45* (7), 2811−2817.

(14) Goldstone, J. V.; Voelker, B. M. Chemistry of Superoxide Radical in Seawater: CDOM Associated Sink of Superoxide in Coastal Waters. *Environ. Sci. Technol.* **2000**, *34* (6), 1043−1048.

(15) Ma, J.; Zhou, H.; Yan, S.; Song, W. Kinetics Studies and Mechanistic Considerations on the Reactions of Superoxide Radical Ions with Dissolved Organic Matter. *Water Res.* **2019**, *149*, 56−64.

(16) Vialaton, D.; Richard, C.; Baglio, D.; Paya-Perez, A.-B. Phototransformation of 4-Chloro-2-Methylphenol in Water: Influence of Humic Substances on the Reaction. *J. Photochem. Photobiol. Chem.* **1998**, *119* (1), 39−45.

(17) Chen, Y.; Zhang, X.; Feng, S. Contribution of the Excited Triplet State of Humic Acid and Superoxide Radical Anion to Generation and Elimination of Phenoxyl Radical. *Environ. Sci. Technol.* **2018**, *52* (15), 8283−8291.

(18) Zhou, Q.; Zhang, X.; Zhou, C. Transformation of Amino Acid Tyrosine in Chromophoric Organic Matter Solutions: Generation of Peroxide and Change of Bioavailability. *Chemosphere* **2020**, *245*, No. 125662.

(19) Bielski, B. H. J.; Allen, A. O. Mechanism of the Disproportionation of Superoxide Radicals. *J. Phys. Chem.* **1977**, *81* (11), 1048−1050.

(20) Cooper, W. J.; Zika, R. G. Photochemical Formation of Hydrogen Peroxide in Surface and Ground Waters Exposed to Sunlight. *Science* **1983**, *220* (4598), 711−712.

(21) Petasne, R.; Zika, R. G. Fate of Superoxide in Coastal Sea Water. *Nature* **1987**, *325*, 516−518.

(22) Powers, L. C.; Miller, W. L. Apparent Quantum Efficiency Spectra for Superoxide Photoproduction and Its Formation of Hydrogen Peroxide in Natural Waters. *Front. Mar. Sci.* **2016**, *3*, 235.

(23) Wuttig, K.; Heller, M. I.; Croot, P. L. Reactivity of Inorganic Mn and Mn Desferrioxamine B with O_2, O_2^-, and H_2O_2 in Seawater. *Environ. Sci. Technol.* **2013**, *47* (18), 10257−10265.

(24) Garg, S.; Rose, A. L.; Waite, T. D. Photochemical Production of Superoxide and Hydrogen Peroxide from Natural Organic Matter. *Geochim. Cosmochim. Acta* **2011**, *75* (15), 4310−4320.

(25) Rose, A. L.; Moffett, J. W.; Waite, T. D. Determination of Superoxide in Seawater Using 2-Methyl-6-(4-Methoxyphenyl)-3,7-Dihydroimidazo[1,2-*a*]Pyrazin-3(7 *H*)-One Chemiluminescence. *Anal. Chem.* **2008**, *80* (4), 1215−1227.

(26) Rusak, S. A.; Peake, B. M.; Richard, L. E.; Nodder, S. D.; Cooper, W. J. Distributions of Hydrogen Peroxide and Superoxide in Seawater East of New Zealand. *Mar. Chem.* **2011**, *127* (1−4), 155−169.

(27) Powers, L. C.; Miller, W. L. Hydrogen Peroxide and Superoxide Photoproduction in Diverse Marine Waters: A Simple Proxy for Estimating Direct CO_2 Photochemical Fluxes: H_2O_2/O_2^- Proxy for CO_2 Photoproduction. *Geophys. Res. Lett.* **2015**, *42* (18), 7696−7704.

(28) Powers, L. C.; Babcock-Adams, L. C.; Enright, J. K.; Miller, W. L. Probing the Photochemical Reactivity of Deep Ocean Refractory Carbon (DORC): Lessons from Hydrogen Peroxide and Superoxide Kinetics. *Mar. Chem.* **2015**, *177*, 306−317.

(29) Shaked, Y.; Harris, R.; Klein-Kedem, N. Hydrogen Peroxide Photocycling in the Gulf of Aqaba. *Red Sea. Environ. Sci. Technol.* **2010**, *44* (9), 3238−3244.

(30) Ma, J.; Nie, J.; Zhou, H.; Wang, H.; Lian, L.; Yan, S.; Song, W. Kinetic Consideration of Photochemical Formation and Decay of Superoxide Radical in Dissolved Organic Matter Solutions. *Environ. Sci. Technol.* **2020**, *54* (6), 3199−3208.
(31) Le Roux, D. Investigation of the Production and Decay Pathways of Superoxide by Chromophoric Dissolved Organic Matter. Ph.D. Dissertation, University of Maryland, College Park, MD, 2022; DOI: 10.13016/ibtq-0fy3.
(32) McDowell, M. S.; Bakac, A.; Espenson, J. H. A Convenient Route to Superoxide Ion in Aqueous Solution. *Inorg. Chem.* **1983**, *22* (5), 847−848.
(33) Bielski, B. H. J.; Cabelli, D. E.; Arudi, R. L.; Ross, A. B. Reactivity of HO_2/O^-_2 Radicals in Aqueous Solution. *J. Phys. Chem. Ref. Data* **1985**, *14* (4), 1041−1100.
(34) Stuever Kaltenbach, M.; Arnold, M. A. Acridinium Ester Chemiluminescence: pH Dependent Hydrolysis of Reagents and Flow Injection Analysis of Hydrogen Peroxide and Glutamate. *Mikrochim. Acta* **1992**, *108* (3−6), 205−219.
(35) Waterville Analytical. *Chemistries*; Waterville Analytical: Waterville, ME, 2018; http://www.watervilleanalytical.com/chemistries.html.
(36) Miller, W. L.; Kester, D. R. Hydrogen Peroxide Measurement in Seawater by (p-Hydroxyphenyl)Acetic Acid Dimerization. *Anal. Chem.* **1988**, *60* (24), 2711−2715.
(37) Canonica, S.; Freiburghaus, M. Electron-Rich Phenols for Probing the Photochemical Reactivity of Freshwaters. *Environ. Sci. Technol.* **2001**, *35* (4), 690−695.
(38) Powers, L. C.; Miller, W. L. Blending Remote Sensing Data Products to Estimate Photochemical Production of Hydrogen Peroxide and Superoxide in the Surface Ocean. *Environ. Sci. Process. Impacts* **2014**, *16* (4), 792−806.
(39) Paul Hansard, S.; Vermilyea, A. W.; Voelker, B. M. Measurements of Superoxide Radical Concentration and Decay Kinetics in the Gulf of Alaska. *Deep Sea Res. Part Oceanogr. Res. Pap.* **2010**, *57* (9), 1111−1119.
(40) Neta, P.; Grodkowski, J. Rate Constants for Reactions of Phenoxyl Radicals in Solution. *J. Phys. Chem. Ref. Data* **2005**, *34* (1), 109−199.
(41) Jonsson, M.; Lind, J.; Reitberger, T.; Eriksen, T. E.; Merenyi, G. Free Radical Combination Reactions Involving Phenoxyl Radicals. *J. Phys. Chem.* **1993**, *97* (31), 8229−8233.
(42) Jin, F.; Leitich, J.; von Sonntag, C. The Superoxide Radical Reacts with Tyrosine-Derived Phenoxyl Radicals by Addition Rather than by Electron Transfer. *J. Chem. Soc., Perkin Trans. 2* **1993**, *9*, 1583.
(43) Winterbourn, C. C.; Kettle, A. J. Radical−Radical Reactions of Superoxide: A Potential Route to Toxicity. *Biochem. Biophys. Res. Commun.* **2003**, *305* (3), 729−736.
(44) d'Alessandro, N.; Bianchi, G.; Fang, X.; Jin, F.; Schuchmann, H.-P.; von Sonntag, C. Reaction of Superoxide with Phenoxyl-Type Radicals. *J. Chem. Soc. Perkin Trans. 2* **2000**, *9*, 1862−1867.
(45) Del Vecchio, R.; Blough, N. V. Photobleaching of Chromophoric Dissolved Organic Matter in Natural Waters: Kinetics and Modeling. *Mar. Chem.* **2002**, *78* (4), 231−253.
(46) Romera-Castillo, C.; Jaffé, R. Free Radical Scavenging (Antioxidant Activity) of Natural Dissolved Organic Matter. *Mar. Chem.* **2015**, *177* (4), 668−676.
(47) King, D. W.; Berger, E.; Helm, Z.; Irish, E.; Mopper, K. Measurement of Antioxidant Activity toward Superoxide in Natural Waters. *Front. Mar. Sci.* **2016**, *3*, 217.
(48) Aeschbacher, M.; Graf, C.; Schwarzenbach, R. P.; Sander, M. Antioxidant Properties of Humic Substances. *Environ. Sci. Technol.* **2012**, *46* (9), 4916−4925.
(49) O'Sullivan, D. W.; Neale, P. J.; Coffin, R. B.; Boyd, T. J.; Osburn, C. L. Photochemical Production of Hydrogen Peroxide and Methylhydroperoxide in Coastal Waters. *Mar. Chem.* **2005**, *97* (1), 14−33.
(50) Sutherland, K. M.; Wankel, S. D.; Hansel, C. M. Dark Biological Superoxide Production as a Significant Flux and Sink of Marine Dissolved Oxygen. *Proc. Natl. Acad. Sci. U. S. A.* **2020**, *117* (7), 3433−3439.

https://doi.org/10.1021/acs.est.3c08254
Environ. Sci. Technol. 2023, 57, 20627−20635